Memorias del XX Congreso Latinoamericano de Control Automático (CLCA 2025)
13-17 de Octubre, 2025. Cancún, Quintana Roo, México

Passivity-Based Controller Applied to a Step-up/Step-down Converter for Battery Discharge Voltage Regulation

Juan A. Villanueva-Loredo * **Diego Langarica-Córdoba** *
Panfilo R. Martinez-Rodriguez * **José S. Murguía-Ibarra** *
Christopher J. Rodriguez-Cortes * **Ángel Hernández-Gómez** *

* *Universidad Autónoma de San Luis Potosí, San Luis Potosí, S.L.P. 78000, México (e-mail: juan.villanueva@uaslp.mx, diego.langarica@uaslp.mx, panfilo.martinez@uaslp.mx, diego.langarica@uaslp.mx, ondeleto@uaslp.mx, cjrcortes@ieee.org, angel.hernandez@uaslp.mx).*

Abstract: In this work, a passivity-based controller for a step-up/step-down converter is designed and validated through numerical results. The proposed control scheme consists of two control loops: an inner loop and an outer loop. The inner control loop is designed using passivity-based control techniques to track the inductor currents through damping injection and energy shaping. Additionally, an uncertainty estimator based on the immersion and invariance (I&I) approach is employed to enhance the robustness of the inner control loop. Meanwhile, the voltage regulation is handled by a PI controller, which maintains the voltage at the desired reference level. The proposed converter and control strategy are well-suited for regulating the voltage fluctuations of lithium-ion batteries when used as the input source to the converter.

Keywords: Passivity-based control, nonlinear control, parameter estimation, DC-DC set-up/step-down converter, lithium-ion batteries.

1. INTRODUCTION

Step-down and step-up converters are common topologies in traditional switching converters (Rahman et al. (2021)). However, with the emergence of new technologies, applications have been identified that require DC–DC converters capable of performing both functions, along with appropriate control schemes. These applications are found in systems powered by photovoltaic panels (Gholizadeh et al. (2023)), battery-powered devices such as electric vehicles (Kim et al. (2019); Cavalcante et al. (2024)), and network devices (Ren et al. (2008)). In all of these applications, an interface is required to manage the output voltage of the power supply, which can vary around its nominal value while supplying a load. Lithium-ion batteries are widely used as power sources for portable devices due to their high energy density (Horiba (2014)). However, the voltage of each battery cell varies from about 4.2 V when fully charged to approximately 2.7 V when discharged (Mishra and De Smedt (2020)). As a result, a DC–DC step-up/step-down converter interface is used between the battery and the load to keep the output voltage at the desired constant level (Mishra et al. (2023)). Furthermore, lithium-ion batteries are recommended not to experience periodic pulse current patterns during discharge, as these sudden fluctuations can be harmful (Savoye et al. (2012)). Therefore, the converter needs to have a smooth, non-pulsating input current, meaning the current does not change suddenly from one level to another. This requirement is fulfilled by including an input inductor in the converter, through which continuous current flow is maintained.

In this paper, a two-loop controller is proposed to regulate the output voltage of a step-up/step-down converter with continuous input current, which is suitable for maintaining a nominal constant voltage for lithium-ion battery applications. Standard passivity-based control (PBC) is used in the inner loop, while a PI controller is employed in the outer loop to achieve output voltage regulation. From a control perspective, this DC-DC voltage regulator presents some challenges because it needs to provide a stable DC output voltage, even when there are changes in input voltage, load conditions, or uncertainties in the system parameters. This PBC method provides a structured approach to designing stabilizing control laws, built around the concepts of energy shaping and damping injection (Komurcugil (2015)). Energy shaping is employed to control the flow of energy within the converter, ensuring that a desired equilibrium point is reached. Subsequently, damping injection is applied to guarantee the asymptotic stability of this equilibrium (Beltrán et al. (2023)). In addition, damping injection is introduced through virtual resistances, which contribute to the stabilization of the system's closed-loop dynamics. Furthermore, an uncertainty estimator based on the immersion and invariance (I&I) approach is employed to enhance the robustness of the inner control loop. This approach is recognized for its effectiveness in designing control laws, state observers, and parameter estimators that ensure asymptotic stabil-

https://doi.org/10.58571/CNCA.AMCA.2025.020

ity in nonlinear systems (Zúñiga-Ventura et al. (2018); Langarica-Cordoba and Ortega (2015)). The performance of the proposed controller has been evaluated and validated through numerical simulations. The main contributions of this work are:

1) A two-loop controller design based on a PI and PBC for a step-up/step-down converter.
2) The development of an uncertainty estimator utilizing immersion and invariance approach.
3) Validation of the proposed regulator through numerical simulation.
4) The proposed converter and control strategy are well-suited for regulating the voltage fluctuations of lithium-ion batteries.

The rest of the paper is organized as follows: In Section 2, a system description of the converter and control objectives are made. In Section 3, the two-loop control strategy is described. In Section 4, simulation results of a 220 V at 500 W regulator are presented. Final remarks are given in Section 5.

2. SYSTEM DESCRIPTION

The proposed converter is shown in Fig. 1. It consists of two inductors, L_1 and L_2, two capacitors, C_1 and C_2, two switches, M_1 and M_2, two diodes, D_1 and D_2, a constant power source E, and a load R. The output voltage is represented by i_O. The steady-state analysis of the proposed converter is developed in Villanueva-Loredo et al. (2025), where the average model is presented as follows:

$$L_1\dot{x}_1 = -x_3 - (1-d)x_4 - R_{L1}x_1 + E, \tag{1}$$

$$L_2\dot{x}_2 = dx_3 - (1-d)x_4 - R_{L2}x_2, \tag{2}$$

$$C_1\dot{x}_3 = x_1 - dx_2, \tag{3}$$

$$C_2\dot{x}_4 = (1-d)(x_1+x_2) - i_O, \tag{4}$$

where $x_1 \triangleq i_{L1}$, $x_2 \triangleq i_{L2}$, $x_3 \triangleq v_{C1}$, and $x_4 \triangleq v_{C2}$. The average control signal is the duty cycle represented by $d \in (0,1)$. According with Villanueva-Loredo et al. (2025), the voltage gain of the converter is

$$\frac{v_{C2}}{E} = \frac{d}{1-d^2}. \tag{5}$$

Notice that with a duty cycle $0 < d < 0.618$, the converter steps down the input voltage, while with a duty cycle $0.618 < d < 1$, the converter steps up the input voltage. The proposed application is to maintain a constant nominal voltage from a Li-ion battery pack; therefore, a control law is required to automatically adjust the duty cycle of the converter.

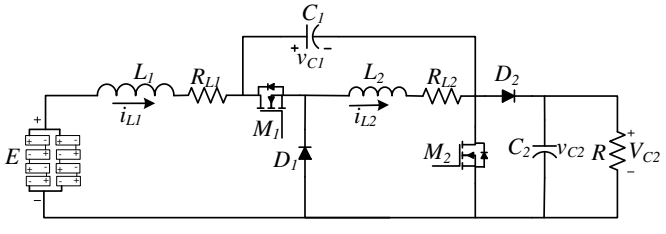

Fig. 1. Proposed step-up/step-down converter.

The control objectives taken into account for designing the control system are:

O1 Inner tracking. To achieve this goal, an inner (PBC) control loop is developed. Through this loop, the state x_i accurately follows the desired state x_i^*. In simple terms, this control objective can be expressed as:

$$\lim_{t\to\infty} x(t) = x^*(t). \tag{6}$$

O2 Output voltage regulation. To achieve this goal, an outer (voltage) loop is implemented to maintain the voltage x_4 constant at a reference voltage V_{ref}. In formal terms:

$$\lim_{t\to\infty} x_4(t) = V_{ref}. \tag{7}$$

To simplify the obtainment of the controller, the following assumptions are considered:

A1 The system is functioning in continuous conduction mode (CCM), which means that the inductor current remains above zero throughout the entire switching period.
A2 All inductance and capacitance values are positive, known, and may change gradually over time.
A3 Active switches and diodes are considered ideal.

3. CONTROLLER DESIGN

In this section, the control law is developed based on the passivity-based control (PBC) principles described in Ortega et al. (1998). The output voltage is regulated indirectly through the inductor current. The control scheme results in two loops: an inner PBC loop and an outer PI control loop. Additionally, to address the issue that the load and parasitic resistance are unknown but constant, an adaptive law grounded in I&I theory is developed (Astolfi et al. (2008)).

3.1 Inner Passivity Based Control Loop Design

In order to develop a suitable model framework for PBC design, the converter dynamics (1) - (4) are represented using the Euler-Lagrange formulation as follows:

$$\mathcal{D}\dot{x} - [\mathcal{J}(d) - \mathcal{R}]\, x = \varepsilon, \tag{8}$$

where $\mathcal{D}$ represents the generalized inertia matrix, the state vector is represented by $x = [x_1, x_2, x_3, x_4]^\top$, $\mathcal{J}(d)$ represents the interconnection matrix with the skew-symmetric property ($\mathcal{J}(d) = -\mathcal{J}(d)^\top$), $\mathcal{R}$ denotes the dissipation matrix, and ε represents an external source vector formed by the input source of the system. In this case, $\mathcal{D}$, $\mathcal{J}$, $\mathcal{R}$ and ε are defined as

$$\mathcal{D} = \begin{pmatrix} L_1 & 0 & 0 & 0 \\ 0 & L_2 & 0 & 0 \\ 0 & 0 & C_1 & 0 \\ 0 & 0 & 0 & C_2 \end{pmatrix}, \tag{9}$$

$$\mathcal{J}(d) = \begin{pmatrix} 0 & 0 & -1 & -(1-d) \\ 0 & 0 & d & -(1-d) \\ 1 & -d & 0 & 0 \\ (1-d) & (1-d) & 0 & 0 \end{pmatrix}, \tag{10}$$

$$\mathcal{R} = diag\{R_{L1}, R_{L2}, 0, 1/R\}, \tag{11}$$

$$\varepsilon = [E, 0, 0, 0]. \tag{12}$$

 https://doi.org/10.58571/CNCA.AMCA.2025.020

The PBC control facilitates the use of energy shaping and damping injection. Energy shaping is used to guide the energy of the converter toward a designated equilibrium point, while damping injection, implemented via virtual resistances, helps maintain exponential stability at that point. To accomplish this, the error state vector is defined as

$$\tilde{x} \triangleq x - x^*. \tag{13}$$

Considering the last definition and the Euler-Lagrange formulation, the following desired dynamics are obtained

$$\mathcal{D}\dot{x}^* - [\mathcal{J}(d) - \mathcal{R}]\, x^* - \mathcal{R}_i \tilde{x} = \varepsilon^*, \tag{14}$$

where $\mathcal{R}_i = diag\{k_1, k_2, k_3, k_4\}$ represents the damping injection component, defined as a diagonal matrix with positive elements k_1, k_2, k_3, and k_4. They can be viewed as virtual resistances that are injected (via feedback) into the converter operation. In addition, ε^* represents the desired input source vector of the system. Therefore, the behavior of the control error dynamics can be determined by analyzing both the dynamics outlined in (8) and the desired dynamics given in (14). This leads to:

$$\mathcal{D}\dot{\tilde{x}} - [\mathcal{J}(d) - \mathcal{R}_d]\, \tilde{x} = \Psi, \tag{15}$$

where the desired dissipation matrix is $\mathcal{R}_d = \mathcal{R} + \mathcal{R}_i$, and $\Psi = \varepsilon - \varepsilon^*$. Furthermore, a closed-loop energy storage function that relies on control error is introduced to help design a control law. This energy storage function is represented as

$$\mathcal{H}_c(\tilde{x}) = \frac{1}{2}\tilde{x}^\top \mathcal{D}\tilde{x}. \tag{16}$$

Observe that $\mathcal{H}_c(0) = 0$, $\mathcal{H}_c(\tilde{x}) > 0\ \forall \tilde{x} \neq 0$, and $\mathcal{H}_c(\infty) \to \infty$ when $||\tilde{x}|| \to \infty$. Additionally, the time derivative of $\mathcal{H}_c(\tilde{x})$ along the error trajectories is represented by

$$\dot{\mathcal{H}}_c(\tilde{x}) = -\tilde{x}^\top \mathcal{R}_d \tilde{x} < 0. \tag{17}$$

Since $\mathcal{R}_d > 0$, the rate of change of $\dot{\mathcal{H}}_c(\tilde{x})$ along the trajectories of the closed-loop system is negative definite. This means that the system is asymptotically stable. The earlier stability analysis, assumes that Ψ remains zero at all times, this is $\Psi = \varepsilon - \varepsilon^* = 0$, which yields to $\varepsilon = \varepsilon^*$. Therefore, according to (8) and (14), to ensure $\Psi = 0$, the control signal d and the auxiliary dynamics for x_2^* to x_4^* are chosen accordingly

$$d = -\frac{1}{x_4^*}\left[E - L_1\dot{x}_1^* - x_3^* + k_1\tilde{x}_1 - x_4^* - \theta_1 x_1^*\right], \tag{18}$$

$$\dot{x}_2^* = \frac{1}{L_2}\left[dx_3^* - (1-d)x_4^* + k_2\tilde{x}_2 - \theta_2 x_2^*\right], \tag{19}$$

$$\dot{x}_3^* = \frac{1}{C_1}\left[x_1^* - dx_2^* + k_3\tilde{x}_3\right], \tag{20}$$

$$\dot{x}_4^* = \frac{1}{C_2}\left[(1-d)x_1^* + (1-d)x_2^* + k_4\tilde{x}_4 - \theta_4 x_4^*\right], \tag{21}$$

where $x_4^* > 0$ since by definition x_4 is positive. The unknown parameters θ_1, θ_2 and θ_4 are redefined as

$$\theta_1 = R_{L1},\ \ \theta_2 = R_{L2},\ \text{ and }\ \theta_4 = \frac{1}{R}. \tag{22}$$

Additionally, the robustness of the proposed controller is enhanced by introducing adaptive I&I theory. The primary goal is the estimation of parasitic resistances linked to the inductors and the load conductance. Based on I&I theory, the estimation error is defined as:

$$z_i \triangleq \theta_i - \hat{\theta}_i, \quad i = 1, 2, 4. \tag{23}$$

Notice that subscript 3 is omitted since no parameter estimation is needed for (3). Furthermore, the estimator is composed of a proportional and an integral part as follows:

$$\hat{\theta}_i = \beta_i + \eta_i(x), \tag{24}$$

where β_i denotes the integral part and η_i denotes the the proportional term. Now, since θ_i includes only constant terms, (23) is expressed as follows:

$$\dot{z}_i = -\dot{\beta}_i - \frac{\partial \eta_i}{\partial x_i}\dot{x}_i. \tag{25}$$

Therefore, if the estimator dynamics are selected as

$$\dot{\beta}_1 = -\frac{1}{L_1}\frac{\partial \eta_1}{\partial x_1}(E - x_3 - (1-d)x_4 - \hat{\theta}_1 x_1), \tag{26}$$

$$\dot{\beta}_2 = -\frac{1}{L_2}\frac{\partial \eta_2}{\partial x_2}(-dx_3 - (1-d)x_4 - \hat{\theta}_2 x_2), \tag{27}$$

$$\dot{\beta}_4 = -\frac{1}{C_2}\frac{\partial \eta_4}{\partial x_4}((1-d)(x_1 + x_2) - \hat{\theta}_4 x_4), \tag{28}$$

and the proportional part is

$$\eta_1 = -\lambda_1 L_1 x_1,\ \ \eta_2 = -\lambda_2 L_2 x_2,\ \ \eta_4 = -\lambda_4 C_2 x_4, \tag{29}$$

then the estimation error dynamics are simplified as:

$$\dot{z}_1 = -\lambda_1 x_1 z_1,\ \ \dot{z}_2 = -\lambda_2 x_2 z_2,\ \ \dot{z}_4 = -\lambda_4 x_4 z_4. \tag{30}$$

The convergence of the estimation error z to zero can be proven by the proposition of a candidate Lyapunov function of the form:

$$V(z) = \frac{1}{2}z^\top z, \quad z = [z_1, z_2, z_4]^\top, \tag{31}$$

where the time derivative along the estimation error dynamics results in

$$\dot{V} = z^\top \dot{z} = -\lambda_1 x_1 z_1^2 - \lambda_2 x_2 z_2^2 - \lambda_4 x_4 z_4^2 \leq 0. \tag{32}$$

Notice that x_1, x_2, and x_4 are positive during nominal operation of the converter. Thus, the control law yields in

$$d = -\frac{1}{x_4^*}\left[E - L_1\dot{x}_1^* - x_3^* + k_1\tilde{x}_1 - x_4^* - \hat{\theta}_1 x_1^*\right], \tag{33}$$

$$\dot{x}_2^* = \frac{1}{L_2}\left[dx_3^* - (1-d)x_4^* + k_2\tilde{x}_2 - \hat{\theta}_2 x_2^*\right], \tag{34}$$

$$\dot{x}_3^* = \frac{1}{C_1}\left[x_1^* - dx_2^* + k_3\tilde{x}_3\right], \tag{35}$$

$$\dot{x}_4^* = \frac{1}{C_2}\left[(1-d)x_1^* + (1-d)x_2^* + k_4\tilde{x}_4 - \hat{\theta}_4 x_4^*\right], \tag{36}$$

The diagram of the proposed control scheme is shown in Fig. 2.

3.2 Outer PI Control Loop Design

After completing the inner PBC loop, the outer PI control is designed to keep the output voltage constant. The output voltage error is

$$e_v \triangleq V_{ref} - x_4 \tag{37}$$

where V_{ref} that denotes the desired voltage reference. The proposed PI control law for output voltage regulation of the converter is

 https://doi.org/10.58571/CNCA.AMCA.2025.020

$$x_1^* = k_p e_v + k_i \phi, \tag{38}$$

$$\dot{\phi} = e_v, \tag{39}$$

where k_p represents the proportional gain and k_i the integral gain of the proposed controller. The auxiliary variable for the integral part is represented by ϕ.

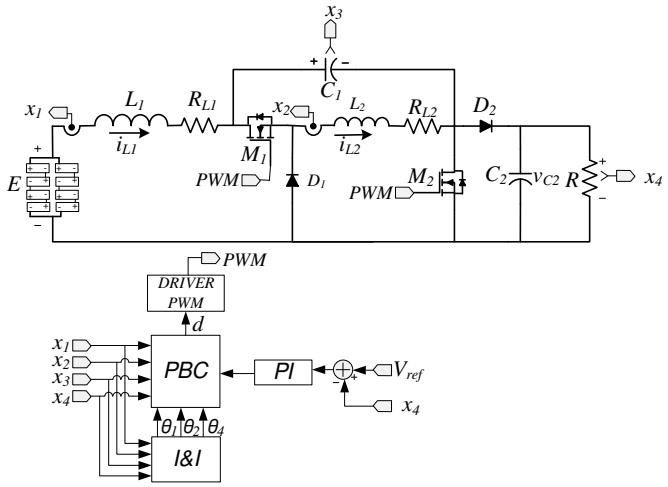

Fig. 2. Diagram of the proposed control scheme.

4. SIMULATION RESULTS

This section showcases the simulation results obtained using PSIM. The converter and controller parameters are listed in Tables 1 and 2, respectively. The input voltage E is assumed to fluctuate between 200 V and 250 V, emulating the behavior of a 220 V Li-ion battery pack with its voltage variation range. The objective is to maintain this voltage at a constant 220 V, ensuring that the load remains unaffected by these voltage fluctuations. To assess the performance in closed-loop, four different test scenarios are considered

a) Steady-state validation,
b) Changes in the input voltage,
c) Step-wise changes in the load,
d) Step-wise changes in the voltage reference.

Table 1. Parameters of the converter.

Parameter	Value
Input voltage E	200 V - 250 V
Voltage reference V_{ref}	220 V
Switching frequency f_s	100 kHz
Inductance L_1	$1.2mH$
Inductance L_2	$1.2mH$
Capacitance C_1	$2.2\mu F$
Capacitance C_2	$2.2\mu F$

4.1 Steady-State Validation

This subsection presents a simulation response of the state variables in steady-state conditions shown in Fig. 3. The nominal input voltage is E=200 V, with a reference voltage V_{ref}= 220 V, and an output power of 500 W. The graph, from top to bottom, shows the input current x_1 and its reference x_1^*, averaging 2.5 A; the current of the second inductor x_2 and its reference x_2^*, averaging 3.9 A; the voltage of the transfer capacitor x_3 and its reference x_3^*, averaging 122 V; and the output voltage x_4 and its references x_4^* and V_{ref}, averaging 220 V. As observed, the output voltage is effectively maintained at the reference value by the proposed control law.

Table 2. Parameters of the controller.

Parameter	Value
Proportional gain K_p	0.1
Integral gain K_i	50
Gain λ_1	100
Gain λ_2	100
Gain λ_4	100
Gain k_1	15
Gain k_2	20
Gain k_3	0.2
Gain k_4	0.1

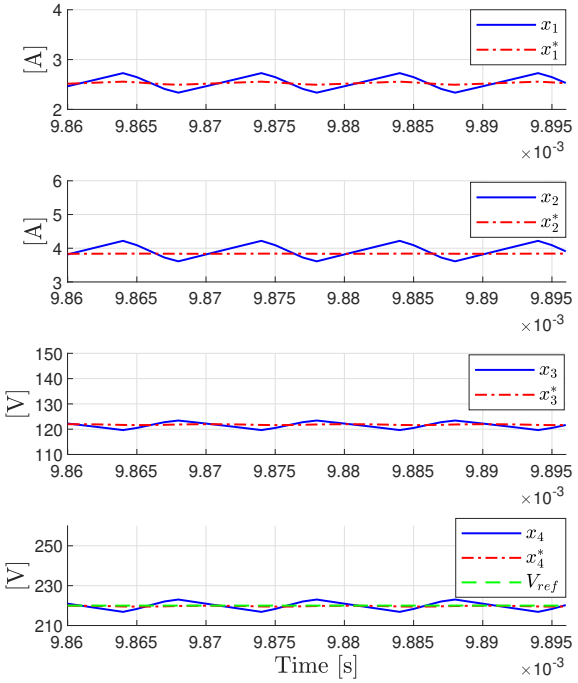

Fig. 3. State variables in steady-state.

4.2 Changes in the Input Voltage

The next test involves changing the input voltage. The voltage reference is fixed to V_{ref} = 220 V. In Fig. 4 the input voltage changes from 200 V to 250 V. This graphic shows from top to bottom: the input current x_1 and its reference x_1^*, which changes from an average value of 2.08 A to 2.38 A; the output voltage x_4 and its references x_4^* and V_{ref}, with an average value of 220 V; the input voltage E, which changes from 200 V to 250 V; and the duty cycle changing from 0.59 to 0.63.

In Fig. 5 the input voltage changes sinusoidally from 200 V to 250 V. This graphic shows from top to bottom: the input current x_1 and its reference x_1^*, which changes sinusoidally from 2 A to 2.5 A; the output voltage x_4 and its references x_4^* and V_{ref}, maintaining an average value of 220 V; the input voltage E, which changes from 200 V to 250 V; and the duty cycle changing from 0.58 to 0.64.

 https://doi.org/10.58571/CNCA.AMCA.2025.020

As observed in both figures, the output voltage remains constant despite variations in the input voltage. Thus, the controller demonstrates adequate performance under these test conditions.

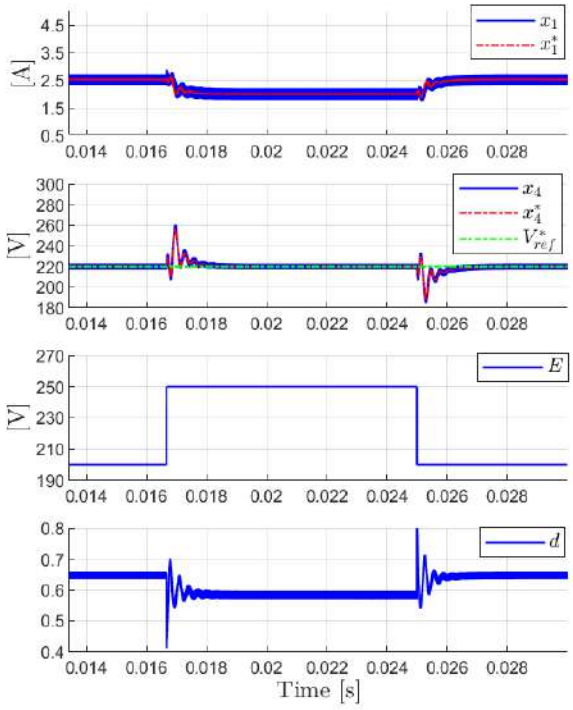

Fig. 4. Step-wise changes to the input voltage from 200 V to 250 V.

4.3 Step-Wise Changes in the Load

The next test involves changing the load in steps from 500 W to 250 W, with an input voltage $E = 250$ V, and a voltage reference $V_{ref} = 220$ V, as shown in Fig. 6. This graphic shows from top to bottom: the input current x_1 and its reference x_1^*, which changes from 2 A to 1 A; the output voltage x_4 and its references x_4^* and V_{ref}, maintaining an average value of 220 V; the output current i_O, which changes from 2.27 A to 1.14 A; and the duty cycle d, which remains around 0.58. The graphic illustrates how the output voltage remains regulated despite load variations.

4.4 Step-Wise changes in the Voltage Reference

The final test involves changing the voltage reference from 200 V to 250 V, as shown in Fig. 7. The input voltage is E= 225 V, and the output power is 500 W. This graphic shows from top to bottom: the input current x_1 and its reference x_1^*, which changes from 1.87 A to 2.93 A; the output voltage x_4 and its reference x_4^*, which accurately follows the established reference changes from 200 V to 250 V; the step-wise change of the voltage reference V_{ref}; and the duty cycle d, which changes from 0.59 to 0.65.

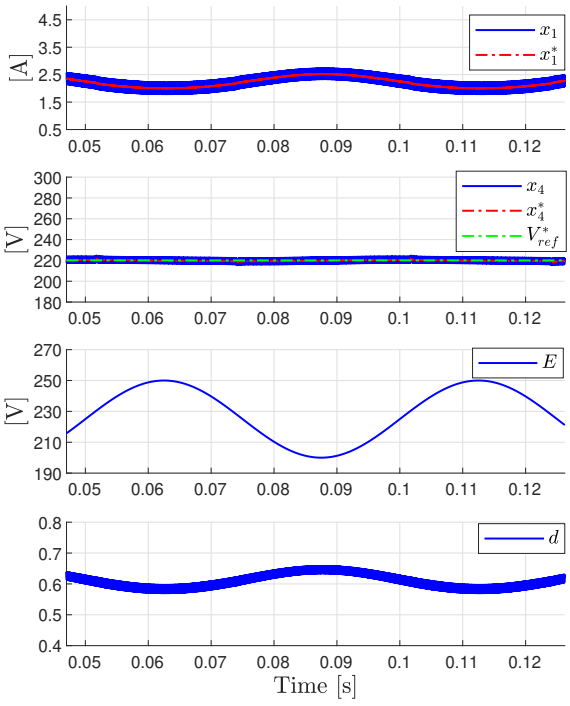

Fig. 5. Sinusoidally changes to input voltage from 200 V to 250 V.

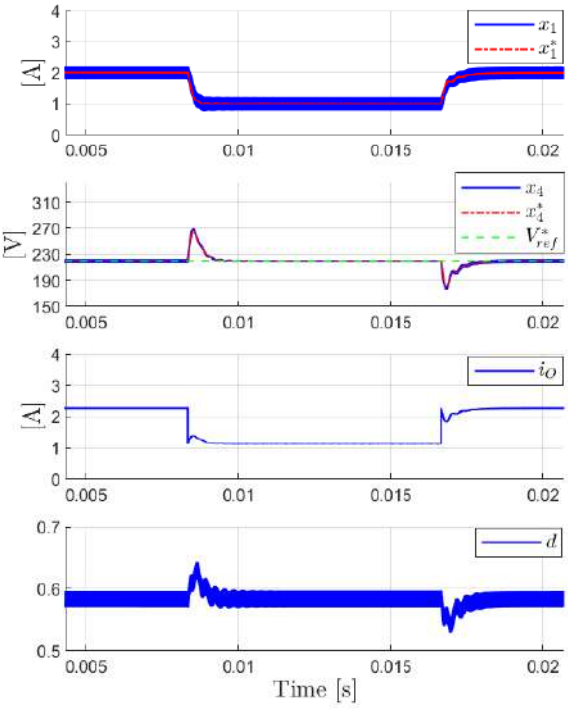

Fig. 6. Step-wise changes to the load from 250 W to 500 W.

 https://doi.org/10.58571/CNCA.AMCA.2025.020

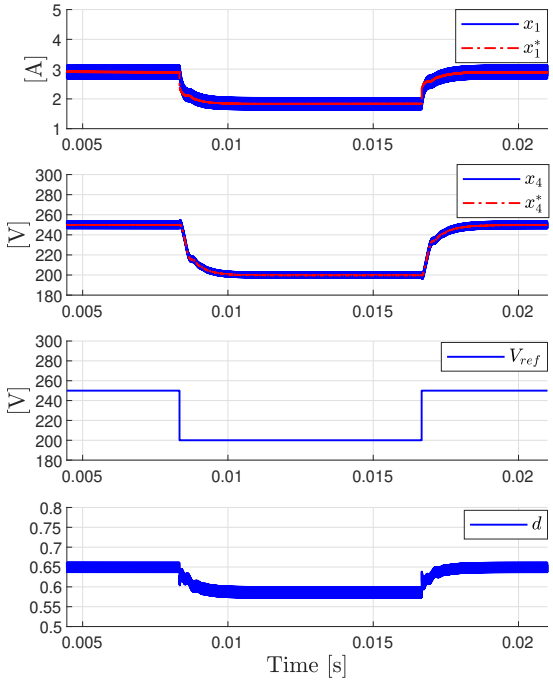

Fig. 7. Step-wise changes in the voltage reference from 200 V to 250 V.

5. CONCLUSIONS

In this paper, passivity-based controller was applied to a step-up/step-down converter. Two independent control loops were designed. The inner control loop was created using standard passivity-based control (PBC) to precisely track the current reference. This current reference is generated by the outer control loop, which employs a PI controller to ensure proper regulation of the output voltage. Moreover, the robustness of the inner loop was enhanced by incorporating an immersion and invariance estimator. To validate the performance of the controller, closed-loop converter simulations were conducted. The input voltage was allowed to vary from 200 V to 250 V, emulating a lithium-ion battery bank with a nominal voltage of 220 V. The converter with the proposed controller was tested in different scenarios, including input voltage changes and load variations. Despite these changes, the converter maintained a constant nominal output voltage. The step-up/step-down voltage characteristics, the continuous input current, and the overall control performance demonstrate that this regulator is suitable for managing the voltage fluctuations of lithium-ion batteries. As future work, an overall stability analysis and experimental results are expected, as well as the consideration of other types of load, such as constant power loads. Finally, a comparison with respect to other types of controllers is envisaged.

REFERENCES

Astolfi, A., Karagiannis, D., and Ortega, R. (2008). *Nonlinear and Adaptive Control with Applications*. Springer, London.

Beltrán, C.A., Diaz-Saldierna, L.H., Langarica-Cordoba, D., and Martinez-Rodriguez, P.R. (2023). Passivity-based control for output voltage regulation in a fuel cell/boost converter system. *Micromachines*, 14(1).

Cavalcante, K.D.N., Kattel, M.B.E., Praça, P.P., Junior, D.S.O., Antunes, F.L.M., and Barreto, L.H.S.C. (2024). 13 kw high-efficiency six-arm high-gain transformerless floating interleaved bidirectional buck–boost dc–dc converter for ev applications. *IEEE Access*, 12, 183901–183917.

Gholizadeh, H., Gorji, S.A., and Sera, D. (2023). A quadratic buck-boost converter with continuous input and output currents. *IEEE Access*, 11, 22376–22393.

Horiba, T. (2014). Lithium-ion battery systems. *Proceedings of the IEEE*, 102(6), 939–950.

Kim, K.D., Lee, H.M., Hong, S.W., and Cho, G.H. (2019). A noninverting buck–boost converter with state-based current control for li-ion battery management in mobile applications. *IEEE Transactions on Industrial Electronics*, 66(12), 9623–9627.

Komurcugil, H. (2015). Improved passivity-based control method and its robustness analysis for single-phase uninterruptible power supply inverters. *IET Power Electronics*, 8(8), 1558–1570.

Langarica-Cordoba, D. and Ortega, R. (2015). An Observer-Based Scheme for Decentralized Stabilization of Large-Scale Systems With Application to Power Systems. *Asian Journal of Control*, 17(1), 124–132.

Mishra, A. and De Smedt, V. (2020). A novel hybrid buck-boost converter topology for li-ion batteries with increased efficiency. In *2020 27th IEEE International Conference on Electronics, Circuits and Systems (ICECS)*, 1–4.

Mishra, A., Zhu, W., Wicht, B., and Smedt, V.D. (2023). An all-1.8-v-switch hybrid buck–boost converter for li-battery-operated pmics achieving 95.63 *IEEE Transactions on Power Electronics*, 38(3), 3444–3454.

Ortega, R., Loria, A., Nicklasson, P.J., and Sira-Ramírez, H. (1998). *Passivity-Based Control of Euler-Lagrange Systems*. Springer.

Rahman, M.D., Nazaf Rabbi, M., and Sarowar, G. (2021). Development of dc-dc converters – a review. In *2021 International Conference on Computational Performance Evaluation (ComPE)*, 341–347.

Ren, X., Tang, Z., Ruan, X., Wei, J., and Hua, G. (2008). Four switch buck-boost converter for telecom dc-dc power supply applications. In *2008 Twenty-Third Annual IEEE Applied Power Electronics Conference and Exposition*, 1527–1530.

Savoye, F., Venet, P., Millet, M., and Groot, J. (2012). Impact of periodic current pulses on li-ion battery performance. *IEEE Transactions on Industrial Electronics*, 59(9), 3481–3488.

Villanueva-Loredo, J.A., Martinez-Rodriguez, P.R., Rodriguez-Cortés, C.J., Langarica-Cordoba, D., Hernández-Gómez, A., and Guilbert, D. (2025). Analysis and control design of a step-up/step-down converter for battery-discharge voltage regulation. *Electronics*, 14(5).

Zúñiga-Ventura, Y.A., Langarica-Córdoba, D., Leyva-Ramos, J., Díaz-Saldierna, L.H., and Ramírez-Rivera, V.M. (2018). Adaptive backstepping control for a fuel cell/boost converter system. *IEEE Journal of Emerging and Selected Topics in Power Electronics*, 6(2), 686–695.

 https://doi.org/10.58571/CNCA.AMCA.2025.020